Tissue mimetic hyaluronan bio-ink containing oriented collagen fibers to modulate hMSC spreading and differentiation

Andrea Schwab[1], Christophe Helary[2], Geoff Richards[1], Mauro Alini[1], David Eglin[1], Matteo D'Este[1]

Author affiliations and contact information
[1] AO Research Institute, Clavadelerstarsse 8, 7270 Davos, Switzerland
[2] Sorbonne Université | UPMC · Laboratoire de Chimie de la Matière Condensée de Paris (LCMCP), Paris

Andrea Schwab
ORCID 0000-0002-4576-558X
andrea.schwab@aofoundation.org

Christophe Helary
ORCID 0000-0001-9312-7278
christophe.helary@upmc.fr

Mauro Alini
ORCID 0000-0002-0262-1412
mauro.alini@aofoundation.org

David Eglin
ORCID 0000-0002-8500-6887
david.eglin@aofoundation.org

Geoff Richards
ORCID 0000-0002-7778-2480
geoff.richards@aofoundation.org

*Corresponding author
Matteo D'Este
ORCID 0000-0002-0424-8172
matteo.deste@aofoundation.org

Abstract

Biofabrication is providing scientists and clinicians the ability to produce engineered tissues with desired shapes, chemical and biological gradients. Typical resolutions achieved with extrusion-based bioprinting are at the macroscopic level. However, for capturing the fibrillar nature of the extracellular matrix (ECM), it is necessary to arrange ECM components at smaller scales, down to the sub-micron and the molecular level.

In this study, we introduce a (bio)ink containing hyaluronan (HA) as tyramine derivative (THA) and collagen (Col). Similarly to other connective tissues, in this (bio)ink Col is present in fibrillar form and HA as viscoelastic space filler. THA was enzymatically crosslinked under mild conditions allowing simultaneous Col fibrillogenesis, thus achieving a homogeneous distribution of Col fibrils within the viscoelastic HA-based matrix. THA-Col composite displayed synergistic properties in terms of storage modulus and shear-thinning, translating into good printability.

Shear-induced alignment of the Col fibrils along the printing direction was achieved and quantified via immunofluorescence and second harmonic generation.

Cell-free and cell-laden constructs were printed and characterized, analyzing the influence of the controlled microscopic anisotropy on cell behavior and chondrogenic differentiation.

THA-Col showed cell instructive properties modulating hMSC adhesion, morphology and sprouting from spheroids stimulated by the presence and the orientation of Col fibers. Actin filament staining showed that hMSCs embedded into aligned constructs displayed increased cytoskeleton alignment along the fibril direction. Based on gene expression of cartilage/bone markers and matrix production, hMSCs embedded into the bioink displayed chondrogenic differentiation comparable or superior to standard pellet culture by means of proteoglycan production (Safranin O staining and proteoglycan quantification) as well as increase in cartilage related genes.

The possibility of printing matrix components with control over microscopic alignment brings biofabrication one step closer to capturing the complexity of native tissues.

1 Introduction

Biofabrication aims at engineering constructs recapitulating the complexity of mammal tissues concerning cell types, chemical and biological gradients, and multiscale architecture.

In extrusion-based 3D printing, the resolution is determined by the size of the nozzle, with resolution ranging from the mm down to the micron range [1]. The physico-chemical properties of the (bio) ink directly influence printing outcome and shape fidelity. The (bio) ink is most often a viscoelastic shear-thinning hydrogel (precursor) with good elasticity recovery after high shear and rapid gelation after extrusion [2-4]. In 3D bioprinting, high resolution must be compromised for cell viability, with typical resolutions in the hundreds of microns range [5]. Thus, for standard extrusion-based techniques, which are the most versatile and widespread, only the macroscopic architecture can be deliberately designed.

By combining different biomaterial ink compositions, gradients of material composition and cellular distribution can be produced using 3D printing techniques [6-8]. Despite impressive advances, the field still lacks reliable methods to mimic tissue architectures at shorter scale lengths [9] and (macro)molecular organization within the biomaterial ink. However, it is well-known how microarchitectural features provide specific and unique properties to every natural tissue [10].

Collagen (Col) is the most abundant protein in the extracellular matrix (ECM), where it is found with a hierarchical fibrillar structure ranging from the triple helix at the molecular level, up to the fibrils and fibers on the microscopic level. Col structure, orientation and spatial arrangement are fundamental towards mechanical stability and anisotropic properties of tissues [11]. The network architecture is also crucial to transmit forces to cells via cell-matrix interaction [12, 13] and contributes to the matrix biochemical environment.

To bring the 3D printing technology one step closer to native tissue architectures, it is necessary to capture micro- and nanostructures within macroscopically complex scaffold geometries [14]. Microarchitectural properties can be introduced with polymer self-assembling, a process where macromolecules arrange into stable non-covalent structures. Col [15], fibrin [12], cellulose [16] and silk fibroin [17] are the most prominent materials self-assembling into fibrous structures.

Most studies printing Col bio(material) inks employ soluble (acidic) and/or non-fibrillar Col inks or blended neutralized Col (Col fractions). Printing an acidic or neutral Col dispersion (2-4% w/v) of swollen Col fibrils with a high viscosity (>10^3 P·s at shear rate of 0.1 1/s) requires subsequent lyophilization and chemical cross linking for scaffold stabilization [18]. Neutralized non fibrillar Col (0.8% w/v) was held at low temperature before extrusion and gelation was induced by printing at 37°C [19]. In another study, neutralized Col fractions were printed at high concentrations (2-4% w/v) and lower temperature (4-15°C) during extrusion printing and gelled within pre warmed media [20].

However, none of these studies investigated the formation and presence of Col fibers within the printed hydrogel construct. Moreover, for all these approaches cell embedding is limited either due to the acidic conditions or the post processing. Another drawback of printing neutralized Col is the phase separation of the self-assembled fibrils from the liquid when extruded [21].

Hyaluronic Acid or hyaluronan (HA) is another fundamental matrix component osmotically capable of holding large amounts of water, and thus functioning as a space filler for fibrillar matrix components, thus providing compressive strength through fluid retention [22]. To our knowledge, methods to control the orientation of Col fibers within a viscoelastic HA-based matrix for bio-fabrication has not been addressed before.

The aim of this study was the development of a THA-Col composite bioink and the workflow to 3D print it, fabricating constructs with homogeneous composition and controlled Col fibril orientation at the microscopical level. In addition, the impact of the microscopic anisotropy on cell behavior of hMSC was analyzed (**Figure** 1). To this aim, the tyramine derivative of HA (THA) was employed to form a continuous matrix where solubilized Col was homogeneously dispersed; THA gelation and Col fibrillogenesis occurred without mutual interference. THA was additionally crosslinked with visible light for final shape fixation, thus achieving a uniform THA matrix containing Col fibrils, which were aligned via the shear forces experienced during the extrusion process. The fibril alignment was quantified and compared to casted constructs. Human mesenchymal stromal cells (hMSC) spheroids were embedded in constructs with different compositions and degrees of alignment to compare their cytoskeleton orientation, sprouting and chondrogenic differentiation.

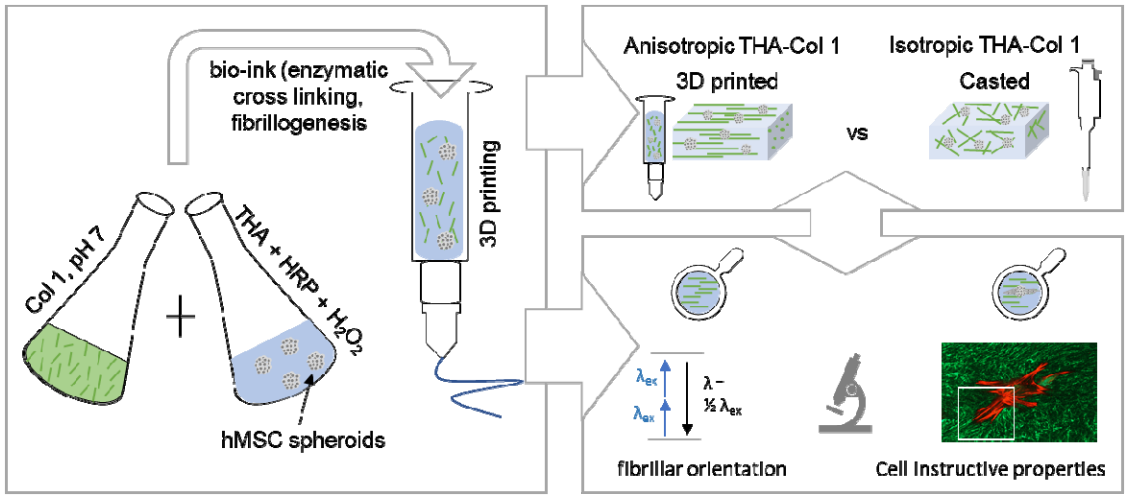

Figure 1: 3D bioprinting as tool to produce microscopic anisotropic scaffolds. *Biomaterial and bio-ink was prepared by mixing neutralized Col (0.5 % w/v) isolated from rat tails with tyramine modified HA (THA, 2.5% w/v). Neutralized Col was mixed with THA for enzymatic crosslinking either cell free or containing hMSC cell spheroids. The Col microstructure was investigated after 3D printing and compared to casted, isotropic samples with different microscopic techniques (SHG imaging and confocal microscopy). Cell instructive properties were analyzed after in vitro culture on cell migration and attachment.*

2 Materials and Methods

2.1 Tyramine modified hyaluronic acid (THA) synthesis

THA was synthesized as previously described [23]. Briefly, HA (280-290 kDa, 5 mM carboxylic groups, Contipro Biotech S.R.O) was functionalized via 4-(4,6-dimethoxy-1,3,55-triazin-2-yl)-4-mehtylmorpholinium chloride (DMTMM, TDI) amidation with tyramine by mixing with a stoichiometric ratio of 1:1:1. Functionalization was performed for 24h at 37°C. THA was precipitated by dropwise by adding Ethanol (96% v/v), isolated with Gooch filter No. 2 and dried. The degree of substitution was 6.6% as determined by absorbance reading at 275 nm (Multiskan™).

2.2 THA-Col hydrogel preparation

THA (2.5% w/v) was reconstituted with minimum Essential Medium alpha (α-MEM, Gibco) supplemented with 10% v/v bovine fetal serum containing peroxidase from horseradish (HRP, Sigma Aldrich) at 4°C under agitation. THA for turbidity measurement was reconstituted with PBS. For light cross linking, 0.02% w/v of EosinY (Sigma Aldrich) was added to THA. Enzymatic cross linking was initiated by adding hydrogen peroxide (H_2O_2, Sigma Aldrich) in different concentrations and incubated for 30 min at 37°C. THA-Col composite was prepared by neutralizing Col 1 (5mg/ml, Collagen I rat tail in 0.2 N acetic acid, Corning) with NaOH and adding to THA before enzymatic cross linking was initiated. Mixing ratios by volumes of THA (2.5% w/v) with Col 1 (0.5% w/v) are given in brackets for all experimental set ups described in the following paragraphs. For cell encapsulation, hMSC spheroids were resuspended with THA before adding H_2O_2. Non-aligned constructs were produced by pipetting the hydrogel precursor with a positive displacement pipette (CP1000, inner diameter ID 1.0 mm, Gilson) into custom made silicon molds (6 mm in diameter). Enzymatic cross linking was performed for 30 min at 37°C.

2.3 3D bioprinting of THA-Col

An extrusion based bioprinter (3D Discovery™, RegenHU) was used to prepare anisotropic hydrogels (0.25" cylindrical needles, 15G: ID 1.36 mm, 0.2 bar, feed rate 8 mm/s; 18G: ID 0.84 mm, 1.6 bar, feed rate 8 mm/s, Nordson EFD) with subsequent light cross linking (515 nm LED, feed rate 4 mm/s). Biomaterial and bio-ink was transferred into 3CC barred (ID 2.3 mm, Nordson) for enzymatic crosslinking (30 min, 37°C), printed with the above-mentioned parameters and transferred into culture media (cell embedded hydrogel) or PBS (cell free).

A complex microstructure to mimic microarchitecture of Col fibers in articular cartilage was accomplished with CAD Software (RegenHU). Fibrillar structure in the superficial zone (SZ at the surface) was realized by printing parallel lines, whereas the Middle (MZ) and deep zone (DZ) by an arch like geometry.

2.4 Rheological characterization

Viscoelastic properties of the biomaterial inks were analyzed using Anton-Paar MCR-302 rheometer with 1° cone-plate geometry and gap distance of 0.049 mm at 20°C. Silicone oil (Sigma Aldrich) was applied to the external border to prevent drying during the measurement. Viscosity was measured with shear rate ranging from 0.01 1/s to 100 1/s to evaluate shear thinning behavior of the enzymatically cross linked (0.3 U/ml HRP, 0.52 mM H_2O_2) THA-Col (1:1 v/v) in a rotational experiment.

Oscillatory tests (amplitude sweep: frequency 1 Hz, amplitude 0.01 - 100% strain; frequency sweep: amplitude 1% strain, frequency 0.01 - 100 Hz) were performed with parallel plate measuring system at 20°C to characterize the elastic modulus of THA and THA-Col at varying polymer concentrations (0.3 U/ml HRP, 0.653 mM H_2O_2).

2.5 Turbidity measurement

Fibrillation of Col was evaluated by absorbance reading at 313 nm at 37°C at 5, 30 and 60 min after gelation ($n \geq 3$) of freshly prepared materials with a Multiskan™ GO Microplate Spectrometer (Thermo Scientific). The following solutions were analyzed: neutralized Col, acidic Col, THA (0.075 U/ml HRP, 0.26 mM H2O2) and THA-Col (1:1 and 1:2 v/v) composite undergoing enzymatic cross-linking during measurement of Col fibrillogenesis.

2.6 Second harmonic generation (SHG) imaging

To visualize Col fibers (0.3 U/ml HRP, 0.52 mM H2O2) (1:1 v/v) SHG images were acquired with a MaiTai multi-photon laser equipped confocal microscope (Leica SP8). SHG signal was collected with HyD detector between 437-453 nm (λ_{ex} 880 nm, output power ap 1.7 W). Additionally, transmitted light and autofluorescence signal (510 - 600 nm) was acquired with varying emission wavelength for SHG detector (λ_{em} 420-436 nm and λ_{em} 454-470 nm) to check for the specificity of SHG signal at 437-453 nm. For deep imaging a long-distance objective (25x water-immersion objective) was used to acquire z-stacks with optimal settings for each sample. Image series acquired with Leica Application Suite X software (LAS X, Leica) were processed with ImageJ (National Institute of health, NIH).

2.7 Cell culture

2.7.1 Cell isolation

hMSCs were isolated from bone marrow aspirate with full ethical approval (Ethics Committee of University of Freiburg Medical Centre (EK-Freiburg: 135/14) as described elsewhere [24]. hMSCs were sub-cultured (3000 cells/cm^2) with α-MEM (Gibco) supplemented with 10% v/v Sera Plus bovine serum (PAN Biotech), 100 U/ml Penicillin, 100 ug/ml Streptomycin (Gibco) and 5 ng/ml basic Fibroblast Growth Factor (FGFb, Fitzgerald Industries International) in a humidified atmosphere of 5% CO_2 with media change every second day.

2.7.2 Cell migration and viability study

Cell spheroids were prepared from hMSC (passage 3-4) in ultra-low attachment petri dish (Corning) with α-MEM media supplemented with 10% bovine serum and 100 U/ml Penicillin, 100 ug/ml Streptomycin before embedded in hydrogels. Cell spheroid suspension was added for (enzymatic) crosslinking (0.3 U/ml HRP, 0.39 mM H_2O_2) into THA-Col (1:1 v/v) or THA or Col 1 at final cell density of 3 Mio/ml and cultured for 8 days.

Live and Dead assay was performed during the migration experiment of hMSC spheroids embedded in enzymatically cross linked (0.3 U/ml HRP, 0.392 mM H2O2) THA-Col (1:1 v/v) with subsequent light cross linking of 3D printed and casted samples at day 1 and 6. After washing with PBS, samples were incubated with 2 µM Calcein AM (Sigma Aldrich) and 1 µM Ethidium homodimer-1 (Sigma Aldrich) for 30 min at 37°C, washed with PBS and imaged using confocal microscope (LSM800, Carl Zeiss). Dead cells were stained with Ethidium homodimer-1 in red (λ_{ex} 561 nm), cytoplasm of living cells was stained with Calcein-AM in green (λ_{ex} 488 nm).

2.7.3 Chondrogenic differentiation

For chondrogenic differentiation, hMSC (passage 2) were seeded in 6 well microwell plate (AggreWellTM 400 plate) at 1.67 Mio/well for 3 days to from cell spheroids. Chondrogenic media is composed of DMEM HG (Gibco) supplemented with non-essential amino acids (1% v/v, Gibco), Ascorbic acid 2 phosphate (50 ug/ml, Sigma Aldrich), Dexamethasone (100 nM, Sigma Aldrich), ITS+ premix (1% v/v, Corning), TGF β1 (10 ng/ml, Fitzgerald) and antibiotics (10 U/ml Penicillin, 10 ug/ml Streptomycin, Gibco). Cell spheroids were embedded in THA-Col (0.5 U/ml HRP, 0.653 mM H_2O_2, 5% w/v Col 1, 1:1 v/v) at final cell concentration of 5 Mio/ml hydrogel volume (400 000 cells/scaffold) before enzymatic gelation and cultured for 21 days with chondrogenic media. Media was changed 3 times a week. For positive control, standard hMSC pellets were prepared by seeding 250 000 hMSCs into each of a 96 V-Bottom well plate (Ratiolab) and cultured under same conditions.

2.8 Histological processing and staining

2.8.1 Actin filament-Col immunofluorescence staining

For actin filament staining in combination with Col 1 immune fluorescent staining, printed and casted THA-Col (1:1 v/v) were fixed for with 4% neutral buffered formalin (Formafix AG) at room temperature and stored in PBS at 4°C upon staining.

Cytoskeletal organization of hMSC sprouting from cell spheroids embedded in enzymatically cross linked THA-Col samples (0.3 U/ml HRP, 0.392 mM H_2O_2) were analyzed on day 0 and after 6 days culture with Phalloidin staining to visualize actin filaments. Hydrogels were permeabilized with 0.5% v/v Triton X-100 (Sigma Aldrich) for 10 min at room temperature, blocked with 10% bovine serum (Sera plus) for 30 min and stained with Phalloidin-TRITC (2 ug/ml, P1951, Sigma Aldrich) for 45 min at room temperature. Immunofluorescence staining for Col 1 was processed directly after phalloidin staining by overnight incubation with primary antibody (COL-1, monoclonal, Sigma Aldrich). Secondary antibody Goat anti mouse, Alexa fluor 488 (Invitrogen) was incubated for 1h. Cell nuclei were stained with DAPI (2 ug/ml, Sigma Aldrich) for 10 min. Samples were washed between every step with Tween-20 (P1379, Sigma Aldrich) 0.1% v/v in PBS and stored in PBS for microscopy.

A confocal microscope (LSM800, Carl Zeiss) was used to acquire fluorescence images (25x, 40x water-immersion objectives) to visualize Col matrix and cells. Col fibers within the hydrogel matrix were stained in green (λ_{ex} 488 nm), cell cytoskeleton in red (λ_{ex} 561 nm) and cell nuclei were stained with DAPI in blue (λ_{ex} 405 nm). For all samples, z-stack images were acquired for single channels and processed with Image J (NIH) to generate 2D z-projection (max intensity). Brightness and contrast settings were adjusted to increase contrast of single-color images. Merged images of single channels were created with the image overlay tool with ImageJ software (National Institute of health, NIH).

2.8.2 Cryo embedding

For histological staining, samples were fixed for 30 min with 4% neutral buffered formalin (Formafix AG) at room temperature and stored, washed with PBS and processed with Sucrose (15% w/v and 30% w/v, Sigma Aldrich) before being embedded in tissue freezing medium (Leica). Samples were cut with a cryostat microtome (HM 500 OM, Zeiss) to 8 µm slices and kept at -20°C until processed for histological staining with Safranin O-Fast Green.

2.8.3 Safranin O-Fast Green staining

To stain the proteoglycans in ECM within hydrogel samples and cell pellets, safranin O staining was performed after 21 days of chondrogenic differentiation. Slides were washed with water to remove the cryo-compound and stained with Weigert`s Haematoxylin (12min, room temperature, Sigma Aldrich), blued with tap water (10min), rinsed with deionized water and stained with Fast Green (0.02% w/v, Fluka) for 6 min to visualize collagenous matrix in green/blue. After washing with acetic acid (1%, Fluka) samples were incubated with safranin O (0.1%, 15min, Polysciences) to stain proteoglycans in red. After washing with deionized water, staining was differentiated with Ethanol (70%, Alcosuisse) and subsequently dehydrated with series of alcohols (ethanol 96%, ethanol absolute, xylene) and cover slipped (Eukitt, Sigma Aldrich). Microscopic evaluation was performed with brightfield microscope (Olympus BX63, Olympus).

2.9 Quantification of cell migration length and area

A sprout morphology tool in ImageJ (NIH) was used to quantify the migration length on phalloidin stained MAX projection images. For bead and sprout detection the mean threshold method was selected with sample specific adjustment of values (Bead detection: blur radius for bead detection 1.0, minimum bead radius 30-110 um, dilate beads by factor 1.0-2.8; Sprout detection: sprout detection radius 1.0 um, minimal plexus area 5000 um^2, minimal sprout area 500 um^2). Migration area was calculated based on resulting black and white mask from Sprout morphology tool results with ROI area measurement. The calculated area includes the area of the cell spheroids.

2.10 Evaluation of Col fiber alignment

2D fast Fourier transform (FFT) of images acquired with SHG and confocal microscopy for Col immunostaining were used for the evaluation of Col fiber alignment. For both microscopic techniques, single channel images at one focus plane were used. The Oval profile plug-in in ImageJ (NIH) was chosen for quantitative evaluation of the Col fiber orientation as detailed described elsewhere [25, 26]. In brief, single images were processed with imageJ (NIH) including unsharp mask, FFT processed, rotated 90°C right, a circular selection with radius 512 made, oval plug in for radial sum executed with number of points 360. The values displayed in the radar plot were grey values normalized to the maximum peak intensity of each single image. For SHG and confocal images, single focus planes were analyzed at three different locations each.

2.11 Gene expression analysis: Real-Time Quantitative Polymerase Chain Reaction (PCR)

Total RNA was isolated from samples (THA-Col, THA-Col MSC and MSC pellet) at day 0, 14 and 21 using TriReagent® (Molecular Research Centre Inc.) following the manufacturers' protocol. RNA quantity was measured with NanoDrop 1000 spectrophometer (Thermo Fischer). cDNA synthesis of 1 ug RNA was performed with Vilo Superscript (Invitrogen) according to manufacturer's protocol. Reverse transcription was carried out with Thermocycler (Mastercycler gradient, Eppendorf) including a pre-heating at 25°C for 10 min, followed by 42°C for 120 min, inactivation of RT for 5 min at 85°C and cooling down to 4°C.

For real time PCR, 10ul of reaction mixture containing TaqMan Universal Master Mix (Thermo Fischer), primer and probes, DEPC water and cDNA was loaded into 384 well plates. PCR was run with an initial heating to 50°C for 2 min, 95°C for 10 min, 40 cycles at 95°C for 15 s with the annealing at 60°C for 1 min.

Relative gene expression of the chondrogenic associated genes Aggrecan (*ACAN*), Col type 2 (*COL2A1*) and *SOX9*, fibrous- and hypertrophy- associated genes (Col type 1 and type X (*COL1A1*, *COL10A1*), *RUNX2* as well as the endogenous control ubiquitin C (*UBC*) were calculated using $2^{-\Delta\Delta Cq}$. The *UBC* housekeeping gene has been proven for stability in the present conditions. Two different controls MSC pellets and MSC embedded in THA-col at day0 were used for the respective samples. Details on the primers and probe sequence as well as catalogue numbers of Assay-on-Demand (Applied Biosystems) are listed in supplementary (**Figure 7**).

2.12 Quantification of Glycosaminoglycans (GAG) and DNA

To quantify GAGs and DNA within MSC pellets and hydrogels, samples were digested with Proteinase K (0.5 mg/ml, Sigma Aldrich) at 56°C. DNA content was measured using Quant-iT™ PicoGreen (Invitrogen) assay according to the manufacturer's instructions. Fluorescence

was measured with a plate reader (Tecan infinite 200 PRO, Tecan) at 485 nm excitation and 535 nm emission including a DNA standard curve. The amount of proteoglycans was determined by dimethylene blue dye method with absorbance measurement at 535 nm including a Chondroitin 4-sulfate sodium salt from bovine trachea (Fluka BioChemika) standard [27]. For calculation of GAGs released into media the cell free THA-Col values were subtracted from the results of hMSC embedded in THA-Col.

2.13 Statistical Analysis

All samples were measured in technical duplicates of n = 2-4 biological replicates per group and time point and displayed as box plot including mean value or as mean values with standard deviation. Statistical analysis was performed with Graph Pad Prism (Prism 8, USA). GAG and DNA content was evaluated using One-way Anova (compare means of each group) with the assumption of no significant differences of SD with Sidak post hoc test to correct for multiple comparisons. Normalization of GAG to DNA as well as PCR data was analyzed using non-parametric Kruskall Wallis test with Dunn's test to correct for multiple comparisons. Statistical significance was assumed for p-values <0.05.

3 Results

3.1 Morphology and mechanical properties of the composite network.

THA-Col composites were prepared dispersing Col into THA, with fibrillogenesis induced by the pH rise and THA crosslinking triggered by H_2O_2 addition. The presence of Col fibers in THA-Col composite hydrogels was characterized by three independent techniques: SHG imaging, confocal microscopy, and turbidimetry (**Figure 2**). As positive control Col hydrogel was included for all measurements. The turbidity measurement allowed evaluating the fibrillogenesis kinetics (**Figure 2 E**). An increase in absorbance (313 nm) over time was observed ranging from 0.4 to 0.8 for THA 1:1 Col and from 0.06 to 1.3 for THA 1:2 Col., indicative of Col fibrillation within the composite. The maximum absorbance values increased with the Col content within the materials. Overall, the highest values around 1.5 were reached for the neutralized Col1 positive control. After 30 minutes of incubation at 37°C a plateau was reached for all groups.

Pure Col in acidic and in neutral solution, and THA showed constant absorbance.

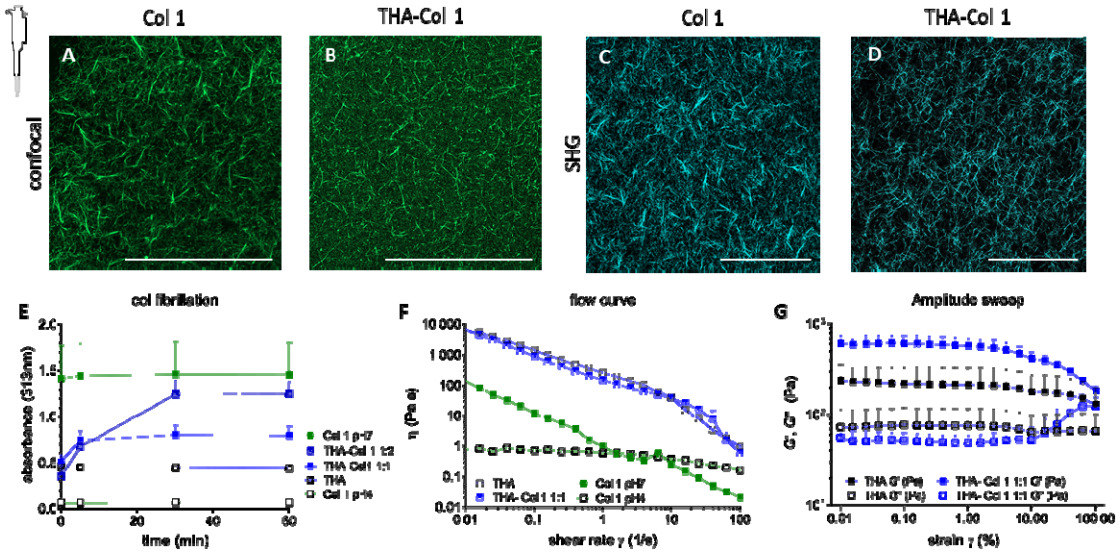

***Figure 2: Collagen fibrils distribution in THA hydrogel and rheological properties**. A) Visualization of Col fibrils within Col hydrogel and B) THA-Col hydrogels using confocal imaging (immunofluorescent staining for Col) and C-D) SHG imaging (no labelling), respectively. Both techniques illustrate homogenous distribution of Col fibrils (scale bar 100 µm). E) Turbidity measurement of THA-Col demonstrated Col fibril formation in composite dependent on Col content. The more Col is present in composite the higher the absorbance at 313 nm over time with maximum values for Col only. F) Flow curve (viscosity as function of shear rate) demonstrate shear thinning behavior of THA, THA-Col and neutralized Col marked by decreasing viscosity with increasing shear rate. Col (pH7, 0.5% w/v) showed lower viscosity compared to THA (2.5 % w/v) and THA-Col. Acidic Col (pH 4, 0.5% w/v) lacks shear-thinning behavior with a constant viscosity over range of tested shear rate. G) Rheological characterization (Amplitude sweep, 1Hz) to evaluate mechanical properties of biomaterial ink by means of storage (G`) and loss (G``) modulus of THA-Col and THA after enzymatic cross linking. Storage modulus increases in composite comparted to THA.*

The fibrillation of Col was further corroborated by imaging. Both SHG imaging (**Figure 2 C**) and confocal microscopy of Col immunofluorescent stained samples (**Figure 2 A**) showed obvious presence of Col fibers with a homogenous distribution within THA. Fiber morphology was visible different, with a thinner and a denser fiber network in THA-Col. Images acquired with confocal and SHG microscopy illustrate identical trend in fibrillar characteristics.
HRP concentration, H_2O_2 content and mixing ratios of THA and Col were selected based on the requirements for rheological properties and extrudability of the biomaterial ink and Col fibrillogenesis. The viscosity curve clearly demonstrated the shear thinning behavior of the biomaterial ink with an overall higher viscosity of 7 kPa for THA-Col and 6 kPa for THA at 0.01 1/s. The viscosity of both inks is decreasing with increasing shear rate up to 10 1/s. At a shear rate higher than 50 1/s the viscosity of THA-Col falls below the value for THA. Neutralized Col (0.5% w/v) resulted in a reduced viscosity ranging from 0.13 k Pas at 0.01 1/s to 1 Pas at 1 1/s. Acidic Col (pH4) showed an evident reduction in shear-thinning with viscosity ranging from 0.8 Pas to 0.6 Pas. Therefore, THA-Col retained the shear thinning behavior required for the biomaterial ink extrusion. An increase in storage modulus was observed in the THA-Col1 composite hydrogel compared to THA (both samples were prepared at the same THA concentration for matching enzymatically cross linking agents (**Figure 2 G**).
The amplitude sweep showed similar profile for THA and THA-Col, with the Col presence implicating an increase in storage modulus, but similar decrease trend at high shear (**Figure 2 G**). This behavior is indicative that THA viscoelastic properties are not disrupted by the formation of the composite with Col.

3.2 Cell instructive properties of THA-Col bioink

hMSCs spheroids were embedded into bio ink made of THA-Col and into its single components to determine how the composition influences cell attachment and sprouting from the spheroids. **Figure 3 A** illustrates a panel of MAX projection images stained for actin filaments on day 0, day 3 and day 8. Cells migrated out of the spheroids into the biomaterials in presence of Col (THA-Col and Col), whereas no migration was observed in THA hydrogels.

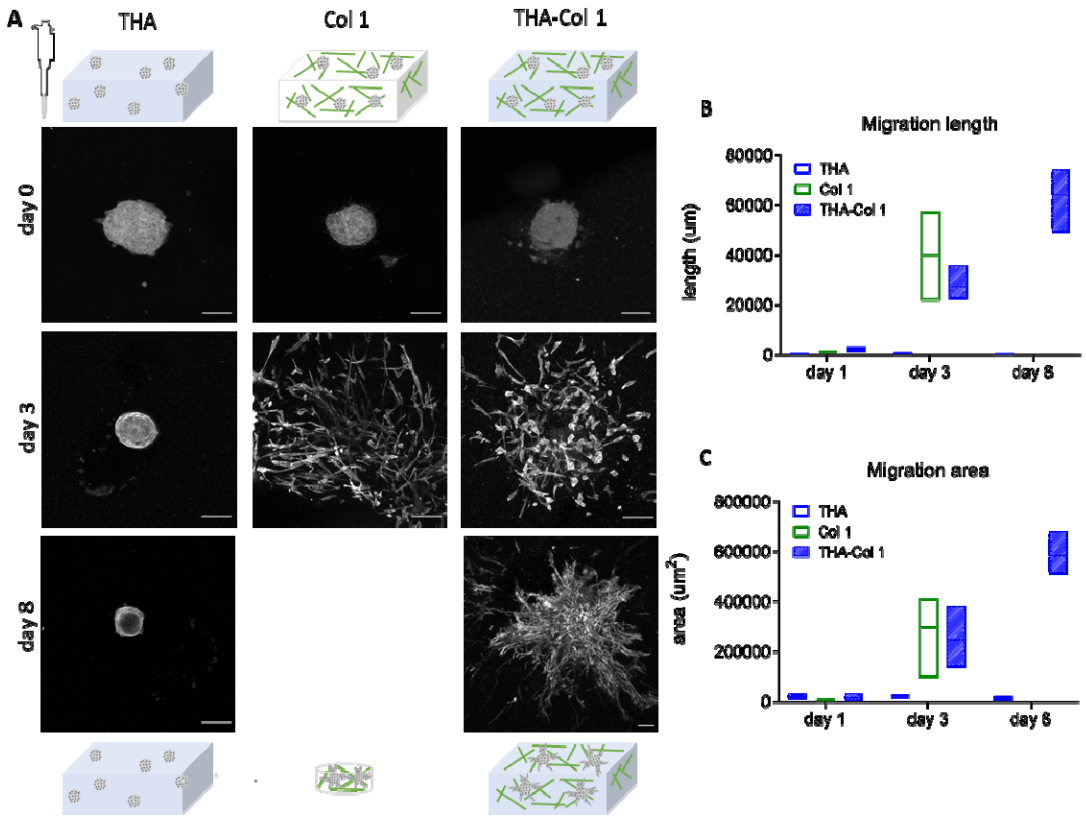

Figure 3: Cell instructive properties of THA-Col addressing hMSC migration and cell attachment*. A) Confocal images of actin filament stained hMSC spheroids embedded in THA-Col (THA-Col, 2.5% w/v 1:1 Col 0.5% w/v), THA (2.5 % w/v) and Col (0.5 % w/v) at day 0, day 3 and after 8 days culture. Migration of hMSC was seen for THA-Col and Col but not in THA. Col hydrogel was shrinking over time and formed a small pellet of less than 2 mm in diameter (Scale bar 100 µm). B) Area of cell migration and C) migration length was higher in Col compared to THA-Col increasing over time. Quantification of migration area and migration length (n=3-5 images).*

Migration length and migration area were quantified with the ImageJ sprout Morphology Tool on MAX projections images stained with phalloidin. Mean values for both parameters confirm the highest migration in Col, followed by THA-Col on day 3. From day 3 to day 8 the migration increased further. In THA, migration area and migration length of hMSC spheroids remained unvaried for the whole duration of the experiment. Due to shrinkage of Col hydrogels and high migration rate, the morphology tool failed to detect the spheroid and to thus quantify the two parameters on day 8 for Col (**Figure 3 B-C**).

3.3 3DP to fabricate microscopically anisotropic scaffolds

After optimizing THA-Col biomaterial ink, the Col presence and fibrillar orientation were characterized. SHG imaging and confocal microscopy were used to visualize the Col fibrils in the THA-Col biomaterial ink after extrusion printing. The fibrillar structure of Col in the composite was preserved after printing and resulted in an anisotropic material. Representative microscopic images in **Figure 4 A and C** clearly demonstrate the presence of parallel aligned Col fibers along the direction of the printing.

To further characterize this property, the ImageJ Oval plug in was used to quantify the alignment of THA-Col after printing and compare to casted THA-Col and casted Col. Casted THA-Col resulted in the least anisotropic properties, followed by casted Col. Comparing the peak width of the preferred orientation in the printed samples (SHG: 120-140 and 300-320,

confocal microscopy: 20-50 and 200-230) to the corresponding casted one (SHG: 40-160 and 220-340, confocal microscopy: 0-180 and 180-360) a clear narrowing of the Col fiber orientation dispersity was observed for the printed sample (**Figure 4 B, D**).

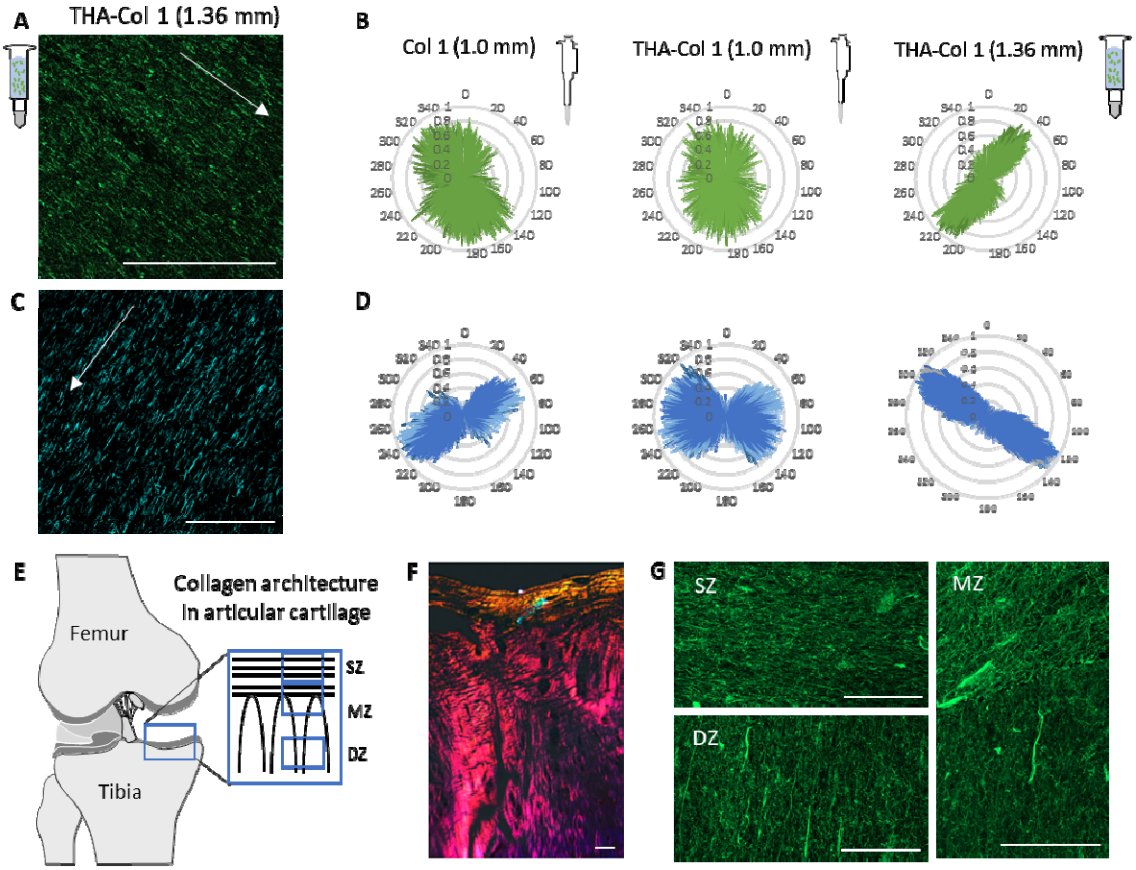

Figure 4: 3DP as tool to align Col fibers and produce microscopically anisotropic scaffolds. *A) Confocal microscopy of immunofluorescent staining against Col 1 and C) SHG images demonstrate anisotropic fibers in THA-Col biomaterial ink (scale bar 100 µm). Unidirectional orientation of parallel Col fibers aligning along the printing direction (white arrow indicated printing direction). B, D) Radar plots display the quantification of fiber alignment in casted Col, casted THA-Col and printed THA-Col (15G: ID 1.36 mm, 0.25" cylindrical needle) from images acquired either with SHG (B, blue) or confocal microscope (D, green). Independently of microscopical method the printed THA-Col samples resulted in unidirectional orientation which was more random for casted THA-Col and Col. E) Schematic illustration of Col fiber alignment in articular cartilage. F) Polarized light image of articular cartilage illustrating horizontal fibers in superficial zone (SZ) and vertical orientation in deep zone (DZ) (scale bar 50 µm). G) 3D Printing was used to produce complex micro structured scaffold (1.4 x 1.6 cm in size, 18G: ID 0.84 mm, 0.25" cylindrical needle) mimicking hierarchical fiber orientation in articular cartilage with parallel horizonal fibers in the SZ, more isotropic fibers in the middle zone (MZ) and parallel vertical fibers in the DZ (scale bar 50 µm).*

The control over the parallel fiber orientation was used to produce a construct imitating the Col orientation in knee articular cartilage. Fibrillar structure in the superficial zone (SZ at the surface) was realized by printing parallel lines, whereas the Middle (MZ) and deep zone (DZ) by an arch like geometry shown in **Figure 4 G** with an overall sample size of 1.4 x 1.6 cm. Immunofluorescent staining against Col clearly show the fibrillar alignment in the three zones with horizontal fibers in the SZ, vertical alignment in the DZ and more isotropic appearance in the MZ.

3.4 Effect of 3DP on cell migration in THA-Col bio-ink

After characterization of the material microstructure and properties, we investigated the response of hMSCs on aligned anisotropic versus isotropic fibers in the THA-Col. The bio-ink was either printed with a cylindrical needle or extruded from the cartridge without needle attached and compared to casted samples. Live/dead staining of hMSC aggregates embedded in THA-Col (printed versus casted) are shown in **Figure 5** over time (day 1, day 6 and day 8). Cells were viable after printing and remained viable over culture time.

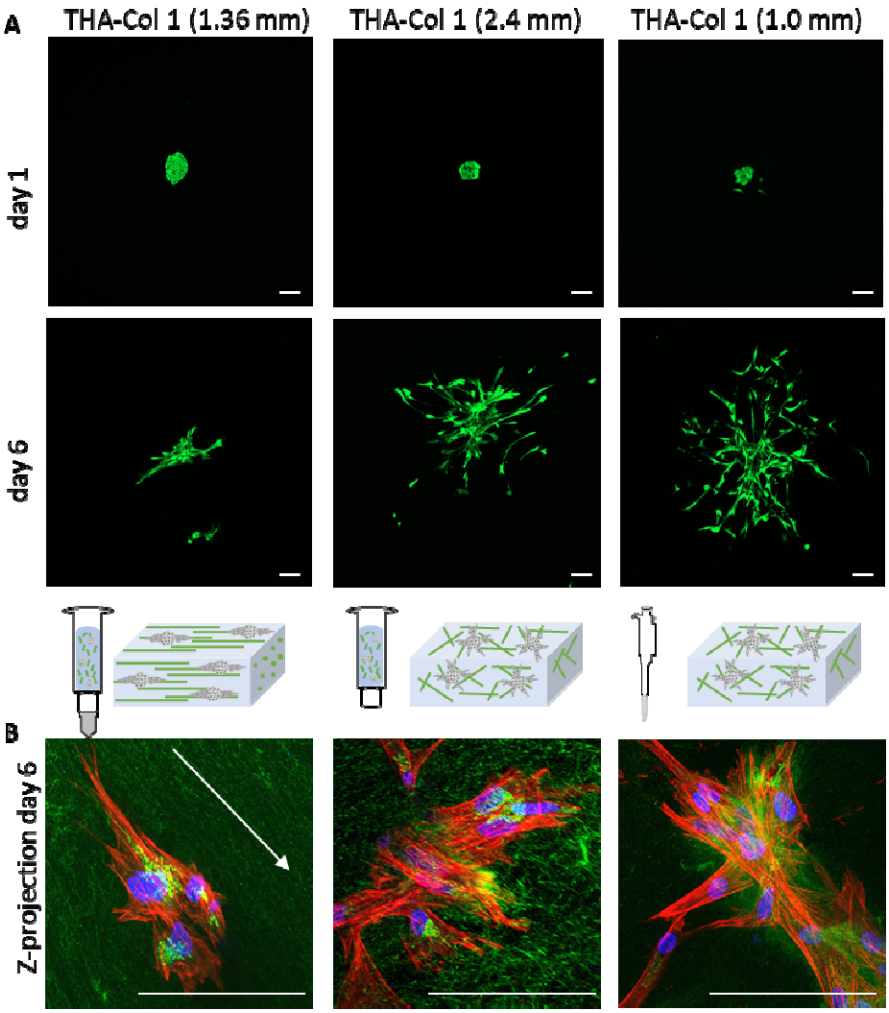

Figure 5: Viability (Live/dead staining) and phalloidin staining of hMSC spheroids in THA-Col hydrogel*. A) Representative images of live/dead staining at day 1 and day 6 showing living cells in green with few dead cells in red (Scale bar 100 µm). Bio-ink was either printed with 15G (ID 1.36 mm) cylindrical needle, extruded from 3CC cartridge without any needle attached or pipetted with CP100 positive displacement pipette. B) MAX z-projection of hMSCs after 6 days of culture in THA-Col1 demonstrating unidirectional actin filaments/cell cytoskeleton (in red) along the Col 1 (green) direction of printed samples (white arrow indicates printing direction) and cell nuclei (blue). In extruded and casted samples cells migrated random in the bio-ink (scale bar 100 µm).*

During *in vitro* culture, hMSC migrated from the spheroids in all three groups. Observing the cytoskeleton orientation via phalloidin staining, MSCs alignment along the printing direction was more pronounced in the printed groups, while hMSC showed a more isotropic cytoskeletal orientation in the extruded and casted group. The overlay image of actin filament

staining (red), cell nuclei (blue) and Col fiber demonstrated the unidirectional migration of the cells along the parallel aligned Col fibers in the printed group (**Figure 5 B**).
Comparing the migration pattern of the extruded and casted group, no differences were observed on day 6 and 8.

3.5 *In vitro* chondrogenic differentiation

Chondrogenic differentiation potential of hMSC spheroids embedded in THA-Col was compared to hMSC pellet culture as positive control, and was evaluated by qPCR, safranin-O staining and total proteoglycan content. Gene expression analysis of hMSCs spheroid embedded in THA-Col (**Figure 6 A**) shows an increase in chondrogenic related markers *COL2A1* (100-1000 fold), *ACAN* (10-100 fold) and *SOX9* (<10 fold) over time similarly to hMSCs pellet. *COL1A1* is slightly down regulated, while *COL10A1* showed an increase of approximately 100 times for the two groups at day 14. At day 21, *COL10A1* stay constant for hMSC embedded THA-Col whereas fold change relative to control sample decreased to <10 for hMSCs pellet. *RUNX2* upregulation was much less pronounced (< 10-fold change) compared to the extracellular matrix associated genes. The ratio *COL2A1/COL1A1* (**Figure 6 B**), was higher for hMSC spheroids embedded in THA-Col (day14: 8.7 ± 3.9 , day21: 57.1 ± 34.2) compared to hMSCs pellet (day14: 1.1 ± 0.8, day21: 3.3 ± 2.5).
At day 21, an increase in proteoglycans resulted for both groups (**Figure 6 C-D**). Total amount of GAGs increased from 0.46 ± 0.38 ug/ml to 4.48 ± 0.13 ug/ml ($p<0.0001$) for hMSCs pellet and from 1.18 ± 0.20 ug/ml to 4.48 ± 0.69 ug/ml ($p<0.0001$) for hMSCs spheroids embedded in the bioink. Release of proteoglycans in the media was 5.88 ± 0.92 ug and 13.58 ± 2.93 ug, respectively. Initial content of proteoglycans in cell free control (THA-Col) of 0.98 ug/ml was released over time into the media. Both groups retained around 25% of the total produced proteoglycans within the sample (MSC pellet 26.8%, THA-Col MSC 23.3%). Normalizing GAG to DNA, values increased for hMSCs pellet within 21 days to 3.88 ± 0.42 ($p=0.0482$) and for hMSCs embedded in THA-Col to 2.34 ± 0.24 ($p=0.0423$).
The histological staining confirmed the chondrogenic differentiation. After 21 days of culture a homogenous distribution of safranin O positive staining was observed for hMSCs pellet and hMSC embedded in THA-Col (**Figure 6 E-F**). The hMSC spheroids were no longer visible in the point of initial seeding because of migration throughout the whole hydrogel resulting in a homogenous cell distribution. No differences in hMSCs morphology were visible comparing the shape of the cells in the pellet to the cells embedded in the hydrogel. Most cells appeared to be condensed (round) with a low population of spindle shaped.
Overall, this experiment pointed out that hMSC embedded in the THA-Col bioink is permissive to cell migration, GAG retention and that it retains the same chondrogenic potential as the gold standard pellet culture.

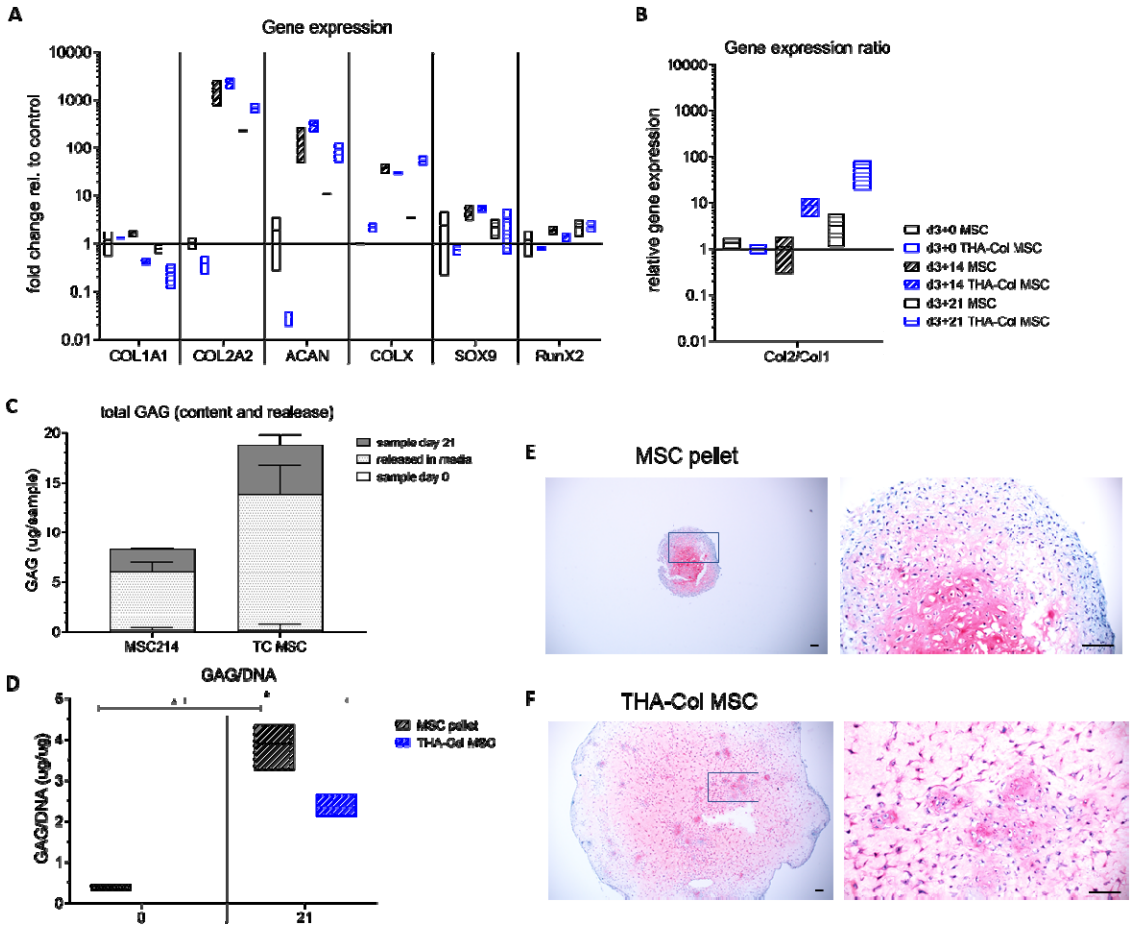

Figure 6: Chondrogenic differentiation potential of hMSC embedded in THA-Col compared to hMSC pellet culture. *A) Gene expression analysis relative to hMSC pellet or hMSC embedded in THA-Col hydrogel (TC MSC) control at day 0 for Col 1 (COL1A1), Col II (COL2A1), aggrecan (ACAN), SOX9 and RunX2. Increase in all chondrogenic related genes with minor changes for SOX9 and RunnX2. B) Relative gene expression ratio of Col II to Col I at day 21. No statistical differences resulted for all PCR data shown. C) Quantification of proteoglycans (GAG/sample) including total amount of GAGs released into the media supernatant and GAGs retained in the sample at day 21. D) GAG/DNA increased over time from day 0 to day 21 for MSC pellet and THA-Col MSC. * p<0.05, **** p<0.0001. E) Safranin O staining to visualize proteoglycans in ECM after 21 days in vitro culture at two magnifications for MSC pellet and F) MSC embedded in THA-Col hydrogel (THA-Col MSC) (scale bar 100 µm).*

4 Discussion

Extrusion-based printing has achieved significant advances in controlling construct resolution, composition and shape. However, the control over the microscopic architecture has been mostly overlooked. Mechanical and biological properties of animal tissues depend not only on the chemical composition, but also on the specific spatial arrangement of structural molecules and biological factors [10]. For example, cartilage is composed of a glycosaminoglycan-based matrix containing Col fibers with specific orientation, parallel to the surface on the superficial zone and perpendicular in deeper layers [28].

In the present work, we propose a technique to introduce anisotropic properties into a THA-Col composite biomaterial. Having two independent cross linking mechanisms, we overcame the difficulty in mixing Col fibrils into a viscoelastic HA-based matrix by combining a previously developed bioink based on the tyramine derivative of HA [29] with acidic-solubilized Col, which was buffered upon mixing, thereby forming fibrils. Since both precursors THA bioink and Col are in liquid form, mixing to homogeneity was easily achieved, as visualized with microscopic techniques. A distinctive advantage of the preparation method here illustrated is that THA crosslinking and Col fibril formation occur simultaneously, thus avoiding phase separation [21].

The preservation of the fibrillar microstructure of low concentrated neutral Col (0.25% final concentration in composite) within THA after 3D printing is a further feature allowing to produce the anisotropic microstructure.

Casted Col hydrogels have been extensively used in the literature, but the fibrillar structure was rarely investigated when combined with a second polymer. Binner *et al.* characterized a star shaped poly (ethylene glycol) hydrogel mixed with Fluorescein-isothiocyanate labelled Col. Besides a homogenous distribution of the Col, no fibrillar structure was shown and further characterized [30].

The shear thinning and viscosity behavior of high concentration neutralized Col (2-6% w/v) has been characterized by different groups [20, 31]. In contrast, 3D printing of neutralized pure Col at low concentrations is challenging due to the lack of shear thinning and shape retention. At the low concentration used in this study (≤ 0.5% w/v), printability was rescued by the shear thinning THA. A similar approach was presented by Duarte Capos *et al.* using agarose as shear thinning component [32]. On the other hand, printing properties of THA previously investigated in our group were preserved upon mixing with Col [33].

The addition of Col to THA increased the storage modulus. Thus, the fibrillar network within the viscoelastic THA can be used as a design parameter to modulate the mechanical properties. Other advantages of the composite are that the cell-mediated shrinking of Col scaffolds is reduced; on the other side, Col provides cell attachment sites to the HA, and an ECM-mimetic fibrillar matrix.

Within the casted gels the fibrils exhibited either random orientation or local domains with some degree of orientation, which could be attributed to the low but non-zero shear forces experienced during casting from a pipette.

After 3D printing of the composite, an overall alignment along the printing axis was observed, as expected. Therefore, the low-grade enzymatic crosslinking of the THA preserved at least in part the capability of the fibrils to comply with the shear stimulus when extruded.

Shear-induced alignment of fibrillar structures has been reported by different groups [34, 35]. Kim *et al.* controlled the fiber alignment in dependence of the needle diameter during printing showing a higher degree of alignment when using 30G compared to 20G needles [34]. This intuitive behavior was not observed in the present study; rather, with thinner needles the fibrillar structure was disrupted, possibly due to the significantly higher pressure that was needed to achieve extrusion, potentially creating discontinuity or turbulence (SI **Figure 7**).

A different approach to align Col fibers was shown by Betsch *et al.* They aligned iron nanoparticle loaded agarose-Col 1 biomaterial ink after exposure to a magnetic field. The alignment was most prevalent in Col 1 (0.3% w/v) compared to the composite (0.3 % w/v agarose: 0.25% w/v Col) only in the group with magnetic field exposure [36]. Yang *et al.* also used electrically assisted printing to mimic Col orientation in meniscus by radial and circumferential aligned carbon nanotubes [37]. With the method here presented, we achieved alignment of Col fibrils within a composite using exclusively natural ECM molecules avoiding

using synthetic non-degradable components simply by 3D extrusion printing. Col only can evolve over time becoming isotropic. This behavior is prevented within the composite, due to the presence of gelled THA stabilizing Col fibrils.

The combination of the two ECM components brings biological features and directs cellular behavior. Single cell seeding resulted in enhanced adhesion, overcoming limited cell attachment reported before [33]. Similar results were observed with cell aggregates, where the presence of Col increased the migration length and area. This behavior can be attributed to presence of the integrin interaction site Arginine, Glycine und Aspartate, (RGD sequence) naturally contained in Col inducing cell adhesion [38]. A direct correlation of cell adhesion and RGD density was shown also for electro spun HA functionalized with RGD peptide by Kim *et al*. [39].

The local microstructure of the material but also fiber parameters regulate cell response [40, 41]. In this study, MSC migration was stimulated along the unidirectional orientation of the Col fibers after 3D printing. In a comparable study, Kim *et al.* showed the unidirectional Actin filament orientation of keratinocytes embedded in corneal stroma-derived decellularized ECM after printing which were less pronounced in non-printed samples for preparation of corneal implants [34]. Yang *et al.* reported an increase in tendon associated genes of rat MSC with oriented Col fiber membrane compared to the isotropic sample [42]. Whether this observation relies on the anisotropic properties or is partially induced by the shear stress during printing is not fully understood.

HA has been attributed a plethora of biological properties, including inducing cell proliferation, chondrogenic differentiation and matrix synthesis [43, 44]. The THA-Col composite here proposed supported the migration and chondrogenic differentiation of hMSC spheroids, resulting in cartilage like matrix deposition throughout the whole hydrogel. Matrix deposition was uniform, with staining comparable to the standard pellet culture control. Importantly, despite Col presence and invasion of the whole matrix, cell morphology was also comparable to the pellet culture, showing a condensed rather than spindle shape morphology. The biomaterial used in this study overcomes the limitation of extracellular matrix deposition only in the pericellular region which is attributed to many seminatural materials used for cartilage tissue engineering.

One possible concern regarding cartilage regeneration is the use of Col type 1 instead of type 2 for our bioink. Clinical studies of a cell free type 1 Col hydrogel (CaReS-1S®, Arthro Kinetics AG) implanted in focal, full layer cartilage defects have shown good clinical outcome addressing defect filling and homogenous structure of the repair tissue [46], with the Col 1 disappearing *in vivo* to leave space to the cell-deposited Col 2 [47]. In a minipig study colonization of the cell free Col matrix gave outcome comparable to matrix assisted chondrocyte implantation [48, 49]. Jiang *et al.* demonstrated superior chondrogenic differentiation of MSC embedded in Col compared to MSC only in a rat model [50]. On the other hand, HA has been combined with Col 1 or gelatin before with similar outcomes that chondrogenic differentiation is promoted in the composite compared to HA or Col only [51-53].

One limitation of the present technique is the shear-induce alignment, limiting the degrees of spatial freedom in fibril arrangement. Another limitation is the missing quantification of the Col fibers within the composite compared to Col hydrogel. This was due to technical limitations in visualizing thin and thicker Col fibers within a 3D hydrogel as a result of autofluorescence, light scattering and opaque hydrogel appearance. For further development, the capacity of regenerating cartilage or other tissues should be tested *in vivo*

interrogating specifically the effect of the orientation separately from the composition, comparing random oriented or non-fibrillar constructs with aligned constructs.

Overall, in this work, we have presented a method to obtain an THA-Col composite with macroscopic homogeneity and microscopic heterogeneity mimicking the macromolecular architecture of native tissues. We achieved a uniform distribution of Col fibers within an HA-based viscoelastic matrix starting from liquid precursors with simultaneous Col fibrillation and HA crosslinking. The orientation of the Col fibers in the 3D printed construct was controlled with the shear stress during printing and had a direct impact on cell behavior. The bioink here introduced can be extended to other fibrillar proteins to produce similar microstructural features. The possibility of printing ECM components with control over microscopic alignment brings biofabrication one step closer to capturing the complexity of biological tissues.

References

1. Murphy, S.V. and A. Atala, *3D bioprinting of tissues and organs.* Nat Biotechnol, 2014. **32**(8): p. 773-85.
2. Hospodiuk, M., et al., *The bioink: A comprehensive review on bioprintable materials.* Biotechnol Adv, 2017. **35**(2): p. 217-239.
3. Melchels, F.P.W., et al., *Development and characterisation of a new bioink for additive tissue manufacturing.* Journal of Materials Chemistry B, 2014. **2**(16): p. 2282.
4. Malda, J., et al., *25th anniversary article: Engineering hydrogels for biofabrication.* Adv Mater, 2013. **25**(36): p. 5011-28.
5. Miri, A.K., et al., *Effective bioprinting resolution in tissue model fabrication.* Lab Chip, 2019. **19**(11): p. 2019-2037.
6. Bittner, S.M., et al., *Fabrication and mechanical characterization of 3D printed vertical uniform and gradient scaffolds for bone and osteochondral tissue engineering.* Acta Biomater, 2019. **90**: p. 37-48.
7. Klein, T.J., et al., *Strategies for zonal cartilage repair using hydrogels.* Macromol Biosci, 2009. **9**(11): p. 1049-58.
8. Nguyen, L.H., et al., *Engineering articular cartilage with spatially-varying matrix composition and mechanical properties from a single stem cell population using a multi-layered hydrogel.* Biomaterials, 2011. **32**(29): p. 6946-52.
9. Heinrich, M.A., et al., *3D Bioprinting: from Benches to Translational Applications.* Small, 2019. **15**(23): p. e1805510.
10. Datta, P., et al., *Anisotropy Properties of Tissues: A Basis for Fabrication of Biomimetic Anisotropic Scaffolds for Tissue Engineering.* Journal of Bionic Engineering, 2019. **16**(5): p. 842-868.
11. Shoulders, M.D. and R.T. Raines, *Collagen structure and stability.* Annu Rev Biochem, 2009. **78**: p. 929-58.
12. Malandrino, A., et al., *Dynamic filopodial forces induce accumulation, damage, and plastic remodeling of 3D extracellular matrices.* PLoS Comput Biol, 2019. **15**(4): p. e1006684.
13. Doyle, A.D. and K.M. Yamada, *Mechanosensing via cell-matrix adhesions in 3D microenvironments.* Exp Cell Res, 2016. **343**(1): p. 60-66.
14. Han, W.M., et al., *Microstructural heterogeneity directs micromechanics and mechanobiology in native and engineered fibrocartilage.* Nat Mater, 2016. **15**(4): p. 477-84.
15. Patel, B., et al., *Self-assembled Collagen-Fibrin Hydrogel Reinforces Tissue Engineered Adventitia Vessels Seeded with Human Fibroblasts.* Sci Rep, 2018. **8**(1): p. 3294.
16. Gladman, A.S., et al., *Biomimetic 4D printing.* Nat Mater, 2016. **15**(4): p. 413-8.
17. Bradner, S.A., et al., *Silk Hydrogel Microfibers for Biomimetic Fibrous Material Design.* Macromolecular Materials and Engineering, 2019. **304**(7): p. 1900045.

18. Lode, A., et al., *Additive manufacturing of collagen scaffolds by three-dimensional plotting of highly viscous dispersions.* Biofabrication, 2016. **8**(1): p. 015015.
19. Diamantides, N., et al., *High density cell seeding affects the rheology and printability of collagen bioinks.* Biofabrication, 2019. **11**(4): p. 045016.
20. Osidak, E.O., et al., *Viscoll collagen solution as a novel bioink for direct 3D bioprinting.* J Mater Sci Mater Med, 2019. **30**(3): p. 31.
21. Rhee, S., et al., *3D Bioprinting of Spatially Heterogeneous Collagen Constructs for Cartilage Tissue Engineering.* ACS Biomaterials Science & Engineering, 2016. **2**(10): p. 1800-1805.
22. Iozzo, R.V. and L. Schaefer, *Proteoglycan form and function: A comprehensive nomenclature of proteoglycans.* Matrix Biol, 2015. **42**: p. 11-55.
23. Loebel, C., et al., *Precise tailoring of tyramine-based hyaluronan hydrogel properties using DMTMM conjugation.* Carbohydr Polym, 2015. **115**: p. 325-33.
24. Gardner, O.F., M. Alini, and M.J. Stoddart, *Mesenchymal Stem Cells Derived from Human Bone Marrow.* Methods Mol Biol, 2015. **1340**: p. 41-52.
25. Tognato, R., et al., *A Stimuli-Responsive Nanocomposite for 3D Anisotropic Cell-Guidance and Magnetic Soft Robotics.* Advanced Functional Materials, 2019. **29**(9): p. 1804647.
26. Ayres, C.E., et al., *Measuring fiber alignment in electrospun scaffolds: a user's guide to the 2D fast Fourier transform approach.* J Biomater Sci Polym Ed, 2008. **19**(5): p. 603-21.
27. Farndale, R., D. Buttle, and A. Barrett, *Improved quantitation and discrimination of sulphated glycosaminoglycans by use of dimethylmethylene blue.* Biochimica et Biophysica Acta (BBA) - General Subjects, 1986. **883**(2): p. 173-177.
28. Buckwalter, J.A., V.C. Mow, and A. Ratcliffe, *Restoration of Injured or Degenerated Articular Cartilage.* J Am Acad Orthop Surg, 1994. **2**(4): p. 192-201.
29. Petta, D., et al., *3D bioprinting of a hyaluronan bioink through enzymatic-and visible light-crosslinking.* Biofabrication, 2018. **10**(4): p. 044104.
30. Binner, M., et al., *Cell-instructive starPEG-heparin-collagen composite matrices.* Acta Biomater, 2017. **53**: p. 70-80.
31. Nocera, A.D., et al., *Development of 3D printed fibrillar collagen scaffold for tissue engineering.* Biomed Microdevices, 2018. **20**(2): p. 26.
32. Duarte Campos, D.F., et al., *Corneal bioprinting utilizing collagen-based bioinks and primary human keratocytes.* J Biomed Mater Res A, 2019.
33. Petta, D., et al., *3D printing of a tyramine hyaluronan derivative with double gelation mechanism for independent tuning of shear thinning and post-printing curing.* ACS Biomaterials Science & Engineering, 2018.
34. Kim, H., et al., *Shear-induced alignment of collagen fibrils using 3D cell printing for corneal stroma tissue engineering.* Biofabrication, 2019.
35. Nerger, B.A., P.T. Brun, and C.M. Nelson, *Microextrusion printing cell-laden networks of type I collagen with patterned fiber alignment and geometry.* Soft Matter, 2019. **15**(28): p. 5728-5738.
36. Betsch, M., et al., *Incorporating 4D into Bioprinting: Real-Time Magnetically Directed Collagen Fiber Alignment for Generating Complex Multilayered Tissues.* Adv Healthc Mater, 2018. **7**(21): p. e1800894.
37. Yang, Y., et al., *Biomimetic Anisotropic Reinforcement Architectures by Electrically Assisted Nanocomposite 3D Printing.* Adv Mater, 2017. **29**(11).
38. Baniasadi, M. and M. Minary-Jolandan, *Alginate-Collagen Fibril Composite Hydrogel.* Materials (Basel), 2015. **8**(2): p. 799-814.
39. Kim, I.L., et al., *Fibrous hyaluronic acid hydrogels that direct MSC chondrogenesis through mechanical and adhesive cues.* Biomaterials, 2013. **34**(22): p. 5571-80.
40. Doyle, A.D., et al., *Local 3D matrix microenvironment regulates cell migration through spatiotemporal dynamics of contractility-dependent adhesions.* Nat Commun, 2015. **6**: p. 8720.
41. Jenkins, T.L. and D. Little, *Synthetic scaffolds for musculoskeletal tissue engineering: cellular responses to fiber parameters.* NPJ Regen Med, 2019. **4**: p. 15.

42. Yang, S., et al., *Oriented collagen fiber membranes formed through counter-rotating extrusion and their application in tendon regeneration.* Biomaterials, 2019. **207**: p. 61-75.
43. Mohan, R., N. Mohan, and D. Vaikkath, *Hyaluronic Acid Dictates Chondrocyte Morphology and Migration in Composite Gels.* Tissue Eng Part A, 2018. **24**(19-20): p. 1481-1491.
44. Amann, E., et al., *Hyaluronic acid facilitates chondrogenesis and matrix deposition of human adipose derived mesenchymal stem cells and human chondrocytes co-cultures.* Acta Biomater, 2017. **52**: p. 130-144.
45. Trentham, D.E., A.S. Townes, and A.H. Kang, *Autoimmunity to type II collagen an experimental model of arthritis.* J Exp Med, 1977. **146**(3): p. 857-68.
46. Efe, T., et al., *Cell-free collagen type I matrix for repair of cartilage defects-clinical and magnetic resonance imaging results.* Knee Surg Sports Traumatol Arthrosc, 2012. **20**(10): p. 1915-22.
47. Schuettler, K.F., et al., *Repair of a chondral defect using a cell free scaffold in a young patient--a case report of successful scaffold transformation and colonisation.* BMC Surg, 2013. **13**: p. 11.
48. Gavenis, K., et al., *Cell-free repair of small cartilage defects in the Goettinger minipig: which defect size is possible?* Knee Surg Sports Traumatol Arthrosc, 2012. **20**(11): p. 2307-14.
49. Schneider, U., et al., *A comparative study of 3 different cartilage repair techniques.* Knee Surg Sports Traumatol Arthrosc, 2011. **19**(12): p. 2145-52.
50. Jiang, X., et al., *The role of Sox9 in collagen hydrogel-mediated chondrogenic differentiation of adult mesenchymal stem cells (MSCs).* Biomater Sci, 2018. **6**(6): p. 1556-1568.
51. Pfeifer, C.G., et al., *Higher Ratios of Hyaluronic Acid Enhance Chondrogenic Differentiation of Human MSCs in a Hyaluronic Acid-Gelatin Composite Scaffold.* Materials (Basel), 2016. **9**(5).
52. Moulisova, V., et al., *Hybrid Protein-Glycosaminoglycan Hydrogels Promote Chondrogenic Stem Cell Differentiation.* ACS Omega, 2017. **2**(11): p. 7609-7620.
53. Yang, J., et al., *Icariin conjugated hyaluronic acid/collagen hydrogel for osteochondral interface restoration.* Acta Biomater, 2018. **74**: p. 156-167.

Acknowledgements

This work is part of the osteochondral defect collaborative research program supported by the AO foundation. The Graubünden Innovationsstiftung is acknowledged for its financial support.

The authors thank Christoph Sprecher for his support with confocal microscopy settings and and Luca Ambrosio for his support setting up the turbidity measurement.

The authors acknowledge support of the Scientific Center for Optical and Electron Microscopy ScopeM of the Swiss Federal Institute of Technology ETHZ for acquiring SHG images.

Additional information

Supplementary information

Table 1: Primer and probe (Forward, reverse and probe sequence) and Assay-On-Demand (Applied biosystem Assay ID) for gene expression analysis.

gene	Forward primer sequence	Reverse primer sequence	Probe sequence	Assay ID
h*ACAN*	5'-AGT CCT CAA GCC TCC TGT ACT CA-3'	5'-CGG GAA GTG GCG GTA ACA-3'	5'-CCG GAA TGG AAA CGT GAA TCA GAA TCA ACT-3'	-

h*COL1A1*	5'-CCC TGG AAA GAA TGG AGA TGA T-3'	5'-ACT GAA ACC TCT GTG TCC CTT CA-3'	5'-CGG GCA ATC CTC GAG CAC CCT -3'	-
h*COL2A1*	5'-GGC AAT AGC AGG TTC ACG TAC A-3'	5'-GAT AAC AGT CTT GCC CCA CTT ACC-3'	5'-CCT GAA GGA TGG CTG CAC GAA ACA TAC-3'	-
h*COL10 A1*	5'-ACG CTG AAC GAT ACC AAA TG-3'	5'-TGC TAT ACC TTT ACT CTT TAT GGT GTA-3'	5'-ACT ACC CAA CAC CAA GAC ACA GTT CTT CAT TCC-3'	-
h*RUNX2*	5'-AGC AAG GTT CAA CGA TCT GAG AT-3'	5'-TTT GTG AAG ACG GTT ATG GTC AA-3'	5'-TGA AAC TCT TGC CTC GTC CAC TCC G-3'	-
h*UBC*				Hs00824723_m1
h*SOX9*				Hs00165814_m1

	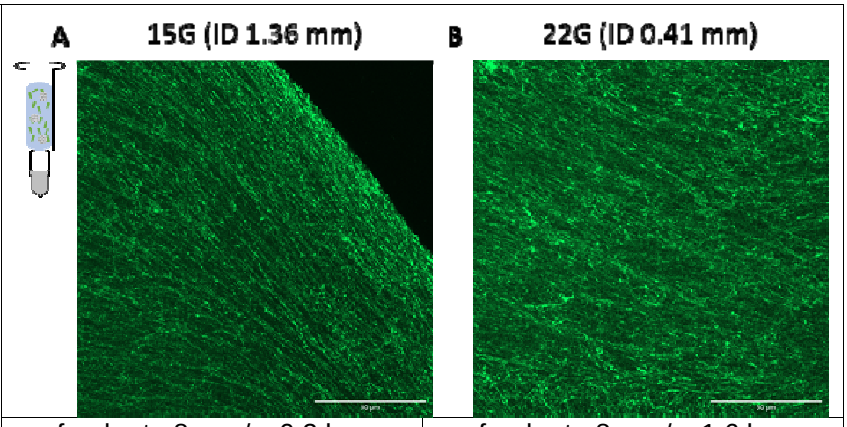	
Printing parameters	feed rate 8 mm/s, 0.2 bar	feed rate 8 mm/s, 1.6 bar

Figure 7: Immunofluorescent staining for collagen I of printed THA-col with 15G (left) and 22G needle including printing parameters. *Orientation of fibers did not display distinct differences. With the thinner needle diameter (22g) the fibers appear to become disrupted compared to the bigger needle diameter (15G). Scale bar 50um.*

Competing interests

The authors declare no competing interests.